Mechanism for material removal in diamond turning of reaction-bonded silicon carbide

Jiwang Yan *, Zhiyu Zhang, Tsunemoto Kuriyagawa

Department of Nanomechanics, Graduate School of Engineering, Tohoku University, Aoba 6-6-01, Aramaki, Aoba-ku, Sendai 980-8579, Japan

ABSTRACT

Reaction-bonded silicon carbide (RB-SiC) is a new ceramic material that has extremely high strength and hardness. Diamond turning experiments were performed on RB-SiC to investigate the microscopic material removal mechanism. Diamond tools with large nose radii of 10 mm were used for machining. It was found that the surface roughness was not significantly affected by the tool feed rate, but was strongly dependent on the tool rake angle. The mechanism for material removal involved plastic deformation, microfracture and dislodgement of 6H-SiC grains. Raman spectroscopy revealed that the silicon bond component underwent amorphization, while no phase transformation of 6H-SiC grains was observed. Tool wear was also investigated and two types of wear patterns were identified. Under the experimental conditions used, a surface finish of 23 nm Ra was obtained even at an extremely high tool feed rate of 72 μm/rev. This study demonstrates the feasibility of precision machining of RB-SiC by diamond turning at a very high material removal rate.

© 2009 Elsevier Ltd. All rights reserved.

1. Introduction

Silicon carbide (SiC) is an important ceramic material that has been extensively used in high-temperature and/or high-pressure applications. For example, in the optical manufacturing industry, SiC is an excellent material for molding dies used for hot-press molding of aspherical glass lenses [1], due to material properties such as high-temperature hardness, thermal shock resistance and chemical stability, which are superior to those of other materials.

The mechanical, thermal and chemical properties of SiC are distinctly dependent on the material manufacturing method. Conventional methods for the manufacture of SiC include pressure-less sintering, gas pressure sintering and hot pressing, where SiC grains are bonded together by a variety of other materials, e.g. boron (B), carbon (C) and aluminum (Al). As a new method, reaction bonding of SiC has become the focus of recent research. Reaction-bonded silicon carbide (RB-SiC) is fabricated by infiltrating silicon (Si) melt into a green compact consisting of C and SiC (mostly 6H-SiC) powders. The liquid Si reacts with the C particles, forming new SiC particles. In this way, a very dense SiC body is produced without the formation of micropores. However, the infiltrated Si melt cannot react with C completely; therefore, excess Si remains in the body of material as a bonding component [2].

RB-SiC has been considered to be a most promising material of the SiC ceramics family. It can be manufactured at relatively low temperatures and with low production costs. It has high purity, dense structure and excellent thermo-mechanical characteristics, such as high thermal stability and conductivity, high specific heat capacity and low thermal expansion. In particular, RB-SiC is characterized by its low density (slightly higher than aluminum) and high stiffness (bending strength over 1000 GPa and Young's modulus higher than 400 GPa). The unique properties of RB-SiC also enable it to be used under cryogenic temperatures, for example, as large-diameter light mirrors of infrared universe imaging systems used in space [3].

However, RB-SiC is typically a difficult material to machine. Recent efforts have focused on the precision machining of RB-SiC by grinding [4,5], lapping [6], polishing [7] and combinations of these. However, to date, there have been no reports on single-point machining (cutting) of RB-SiC. RB-SiC is harder than most other materials except diamond, cubic boron nitride (cBN) and boron carbide (B_4C) [8], and hence available cutting tool materials for machining RB-SiC are very limited. Investigation of the machinability of RB-SiC using ultra hard cutting tools is therefore a challenging issue. If successful methods for precision cutting of RB-SiC can be developed, then extensive industrial applications of RB-SiC can be expected. Compared with abrasive machining processes, cutting has higher material removal rates and higher flexibility when fabricating complicated shapes and microstructures.

The aim of the present work is to investigate the machinability of RB-SiC by precision cutting tests using a single-crystal diamond tool. The machining mechanisms were investigated with respect to surface topography, microstructural changes, chip formation

* Corresponding author. Tel.: +81 22 795 6946; fax: +81 22 795 7027.
E-mail address: yanjw@pm.mech.tohoku.ac.jp (J. Yan).

and tool wear characteristics. Emphasis was placed on the effects of tool feed rate and tool rake angle in this investigation. The cutting phenomena observed for RB-SiC were also compared with our previous works on the precision machining of Si and germanium (Ge). It is expected that the present study will provide feasible evidence for the partial or complete replacement of abrasive machining processes with diamond turning in the fabrication of precision micro RB-SiC parts.

2. Experimental details

2.1. Machining apparatus

Diamond turning experiments were carried out on a numerically controlled three-axis ultraprecision lathe, the configuration of which is schematically shown in Fig. 1. The lathe has two perpendicular hydrostatic tables along the X- and Z-axis directions, in addition to a B-axis rotary table built into the X-axis table. Both X-axis and Z-axis tables have linear resolutions of 1 nm, and the B-axis rotary table has an angular resolution of one ten-millionths of a degree. Prior to machining, the sample was bonded onto a copper blank using heat-softened wax and the blank was then vacuum chucked onto an air-bearing spindle. Thus the sample can be rotated with the spindle and moved along the Z-axis direction, while the cutting tool can be moved along the X-axis direction and also rotated around the B-axis.

2.2. Diamond tool

Conventionally, round-nosed diamond tools have been used for the ductile machining of brittle materials with a tool nose radius of less than 1 mm, or even much smaller [9,10]. To obtain a crack-free surface using this type of tool, the tool feed rate must be extremely low (1–3 μm/rev), and as a result, the material removal rate is very low. In order to realize high-efficiency ductile machining, a straight-nosed diamond tool has been proposed for ductile machining [11], which enables an extremely high material removal rate to be achieved in the ductile mode by using a sufficiently small cutting edge angle. The straight tool has been successfully used in the fabrication of convex aspherical and Fresnel lenses of Si and Ge on numerically controlled 3-axis machining tools [12]. However, it is sometimes difficult for straight tools to fabricate concave surfaces due to tool–workpiece interference. To solve this problem, we previously conducted a study into the ductile machining of Ge using round-nosed diamond tools with large radii up to a several tens of millimeters [13], and the material removal rate was improved by 15 times compared to that of conventional round tools.
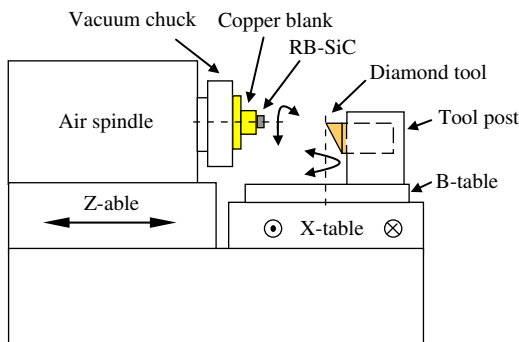

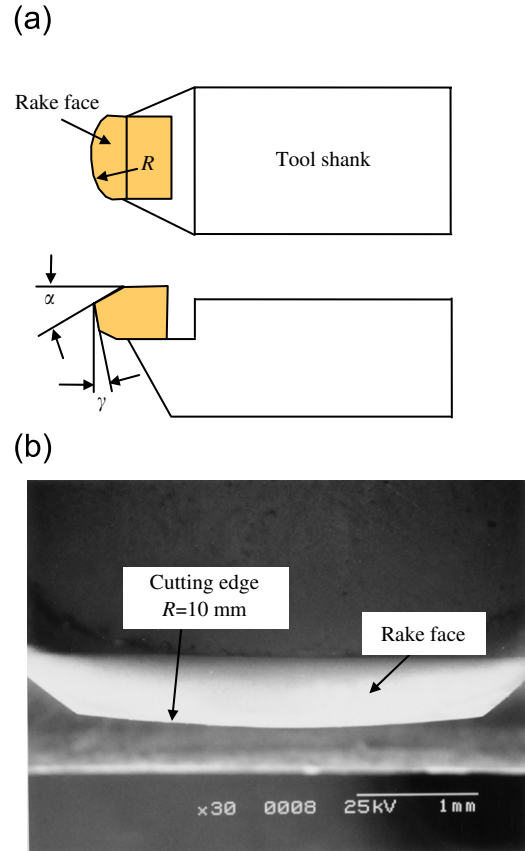**Fig. 1.** Schematic diagram of the ultraprecision machine tool used in cutting experiments.

Fig. 2. (a) Schematic diagram and (b) SEM micrograph of a large nose-radius diamond tool.

In this work, round-nosed diamond tools with 10 mm nose radius were used for cutting RB-SiC. Fig. 2(a) presents a schematic diagram of the diamond tool where α and γ are the tool rake angle and the tool relief angle, respectively. Fig. 2(b) shows a scanning electron microscope (SEM) micrograph of the tool. When cutting with a round-nosed tool, the maximum undeformed chip thickness t_{max} is an important parameter for evaluation of the cutting performance. t_{max} can be calculated from the tool nose radius R, depth of cut d and tool feed rate f, as shown in Fig. 3. When $f \geqslant \sqrt{2Rd - d^2}$, as shown in Fig. 3(a), t_{max} is equal to the depth of cut d; and when $f < \sqrt{2Rd - d^2}$, as shown in Fig. 3(b), t_{max} is given by

$$t_{max} = R - \sqrt{R^2 + f^2 - 2f\sqrt{2Rd - d^2}}. \tag{1}$$

In the present work, $R \gg f$ and $R \gg d$; therefore, Eq. (1) can be simplified as follows:

$$t_{max} \approx \frac{f}{R}\sqrt{2Rd - d^2} \approx f\sqrt{\frac{2d}{R}}. \tag{2}$$

2.3. RB-SiC samples and material properties

The RB-SiC samples used in these experiments were produced by Japan Fine Ceramics Co., Ltd. The as-received samples were cylinders with diameter of 30 mm and thickness 10 mm. Some typical material properties of the sample are as follows: elastic modulus $E = 407$ GPa; bending strength $R_T = 780$ GPa and density $\rho = 3.12$ g cm^{-3}. The volume ratio of residual Si bond is 12%, and the average size of the 6H-SiC grains is less than 1 μm.
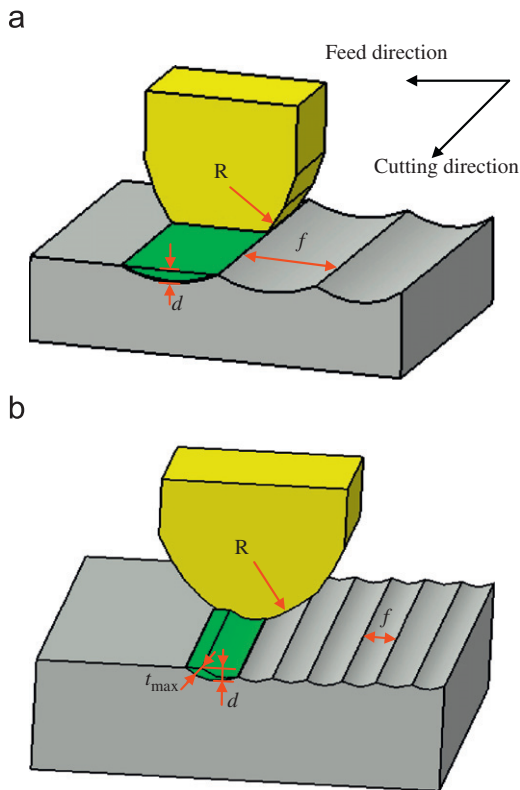
Fig. 3. Schematic model of the maximum undeformed chip thickness t_{max} for cutting with a round-nosed tool when (a) $f \geqslant \sqrt{2Rd - d^2}$ and (b) $f < \sqrt{2Rd - d^2}$.
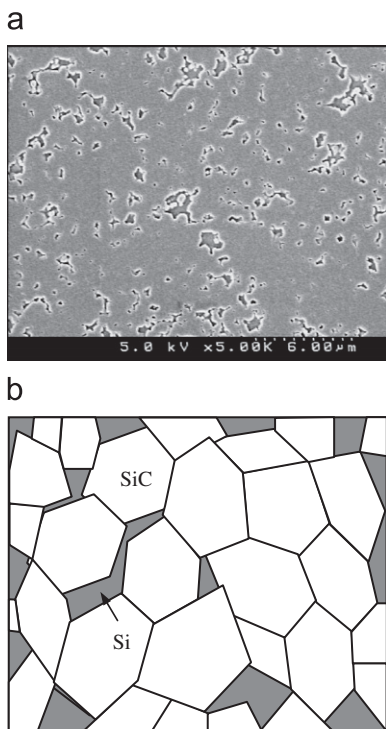

Fig. 4. (a) SEM micrograph of a FAB surface-etched RB-SiC sample. The smooth region is SiC and the micropits correspond to the Si bond. (b) Schematic model of the RB-SiC material microstructure.

In order to clarify the microstructure, the surface of a sample was etched for 15 min using a fast atom beam (FAB) source with SF_6 as a process gas. Fig. 4(a) shows an SEM micrograph of the etched

Table 1
Machining conditions.

Workpiece material	RB-SiC
Tool material	Single-crystal diamond
Tool radius R	10 mm
Rake angle α	0°, −40°
Relief angle γ	10°
Depth of cut d	2 μm
Spindle speed v	2000 rpm
Tool feed rate f	0.1–72 μm/rev
Maximum undeformed chip thickness t_{max}	2–1440 nm
Cutting environment	Dry

surface. Since the etching rate of Si is much higher than that of SiC, the Si bond on the surface was etched deeper than SiC, resulting in the formation of micropits. The SiC grains (smooth region) and Si bond (corresponding to the micropits) can be clearly identified in the micrograph. The sizes of intergrain residual Si bond portions are less than 1 μm, and most of the SiC grains are directly bonded to each other without the presence of Si at the grain boundaries. Fig. 4(b) presents a schematic model of the RB-SiC microstructure. In the material, the newly reaction-generated SiC grains are closely combined to the originally existing SiC grains, resulting in a very dense structure.

These results indicate that the microstructure of RB-SiC is distinctly different from those of single-crystal SiC and SiC prepared by chemical vapor deposition (CVD). Single-crystal SiC has a uniform crystalline lattice structure across the entire wafer. CVD-SiC has polycrystalline or amorphous structure, depending on the deposition conditions used. However, both single-crystal SiC and CVD-SiC are single-phase materials with extremely high purity. Therefore, it can be presumed that the cutting mechanism of RB-SiC, which is a two-phase compound material having a major phase of high hardness (SiC) and a minor phase of low hardness (Si), will be distinctly different from those of single-crystal SiC wafer [14] and CVD-SiC [15]. It will be also different from those of multi-phase materials such as particle-reinforced metal matrix composites (MMCs), which are composed of a major phase of low-hardness matrix and a minor phase of reinforcing particles embedded in the matrix [16–18].

2.4. Machining conditions and surface characterization methods

Face turning was performed on the end faces of the samples. The detailed machining conditions are listed in Table 1. After machining, the resulting workpiece surfaces were evaluated in terms of surface roughness/topography and material microstructural changes. The surface roughness was measured using a contact-type stylus profilometer (Form Talysurf 6, Taylor Hobson), and the material microstructural change was examined using a laser micro-Raman spectrometer (NRS-2100, Jasco). The laser wavelength in the Raman system was 532 nm and the nominal spot size of the laser was 1 μm. Samples of machined specimens were Au–Pd coated for 30 s and the surface damage was examined using SEM. SEM observation of the cutting chips was also performed to assist clarification of the material removal mechanisms, and the cutting tools were also examined to evaluate tool wear patterns.

3. Results and discussion

3.1. Effects of tool feed rate

Firstly, a tool with a 0° rake angle was used for cutting to examine the effect of t_{max} on the surface roughness and the

topography. From Eq. (2), it is known that for a given tool nose radius, both f and d change t_{max}. In the cutting test, the spindle speed v was set at 2000 rpm and d was set to 2 μm. Feed rates were gradually changed from 3 to 72 μm/rev, and thus the t_{max} varied from 60 to 1440 nm.

Fig. 5 shows a surface profile of the machined sample. Even though the tool feed rate was increased by a factor of 24 (from 3 to 72 μm/rev), the surface height peak-to-valley showed little change and was maintained approximately 0.2–0.3 μm, which indicates that the tool feed rate has a negligible effect on the surface roughness. This result is distinctly different from that for cutting Si [11], where beyond a critical undeformed chip thickness, the
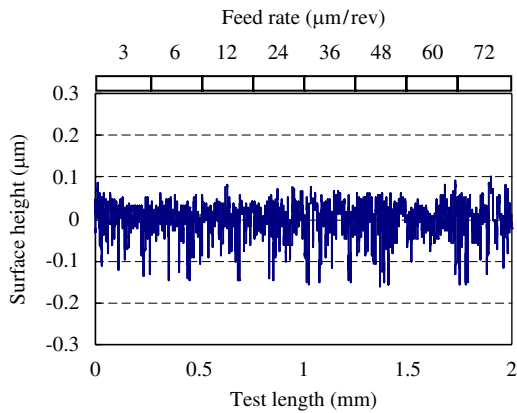
surface roughness is significantly increased due to the occurrence of cleavage fractures.

Fig. 6(a) and (b) show two SEM micrograph pairs (at different magnifications) of the surfaces machined at the lowest (3 μm/rev) and highest (72 μm/rev) tool feed rates, respectively, using a tool rake angle of 0°. In Fig. 6(a), periodical tool feed marks are observed on the surface. Although the majority of the surface is smooth and exhibits a ductile-cut appearance, a few small pits whose sizes are in the order of 1 μm, similar to that of the SiC grains, are clearly observed. Therefore, these micropits may have been caused by the dislodgement of SiC grains from the surface [19].

In contrast to Fig. 6(a), no periodical tool feed marks are observed in Fig. 6(b). This is because the tool feed rate is very high (72 μm/rev) in this case and the field of view is between two neighboring feed marks. Both the size (average 2 μm) and the number of micropits have increased compared with those in Fig. 6(a). However, no brittle fractures as large as a few tens of microns, which are often seen in the machining of single crystalline materials such as Si and Ge in brittle mode, were observed.

3.2. Effects of tool rake angle

Rake angle α is known to be a key parameter in the diamond turning of brittle materials, such as Si and Ge. A negative rake angle is important for ductile regime machining, because it can produce a compressive stress field, which is beneficial for the removal of ductile regime material. In Si wafer machining, the optimal rake angle α has been demonstrated to be approximately
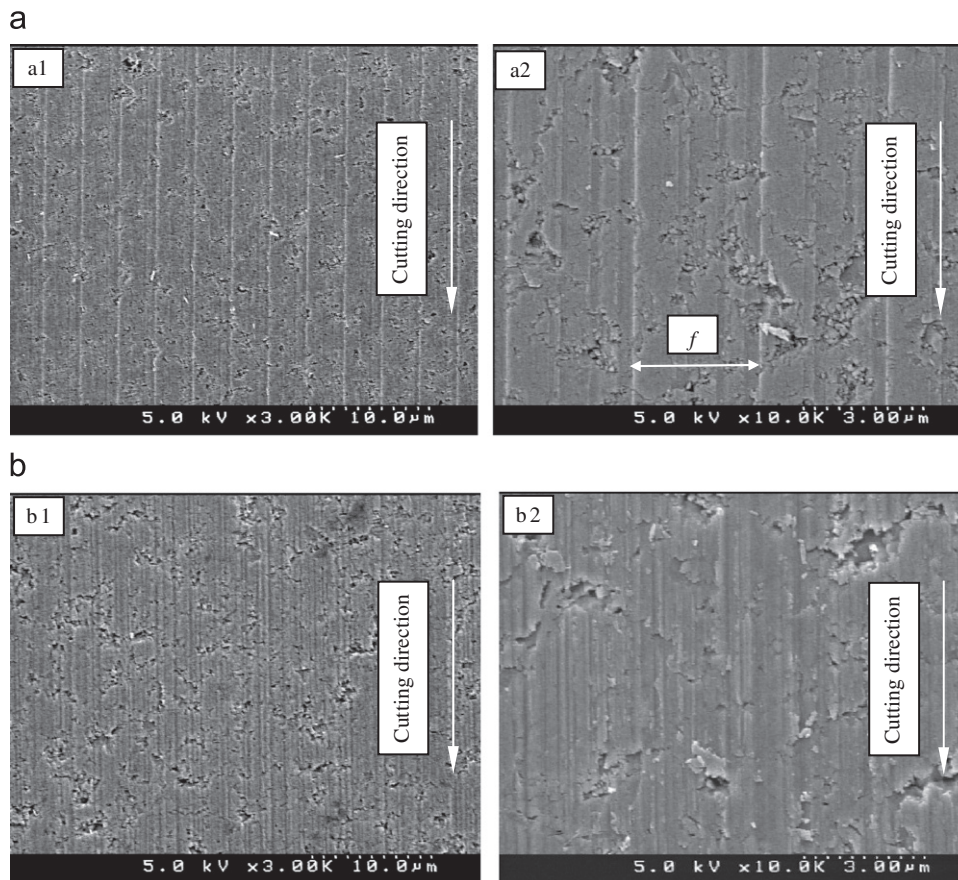
Fig. 5. Surface profile of a sample machined using 0° rake angle tool when the tool feed is varied from 3 to 72 μm/rev.

Fig. 6. SEM micrographs of surfaces machined at (a) $f = 3$ μm/rev and (b) $f = 72$ μm/rev, using 0° rake angle tool. The micrograph pairs were obtained at different magnifications.

−40° [20]. In the present experiments, 0° and −40° rake angle tools were used for turning the RB-SiC sample. For each tool rake angle, the tool feed rates were gradually increased from 0.1 to 72 µm/rev, and hence t_{max} was also increased from 2 to 1440 nm.

In order to evaluate the effects of tool rake angle on the machining performance, a new parameter, the fracture ratio k, was introduced to indicate the extent of microfractures. SEM micrographs of the machined surfaces were processed using the commercially available software (Photoshop®, Adobe Systems Incorporated). As shown in Fig. 7, by counting the total number of pixels for the fractured areas (P_{Ai}, $i = 1, 2, 3,...$) and that of the entire micrograph (P_{A0}) using the histogram palette in the software, k can be described as

$$k = \frac{\sum\limits_{i=0}^{\infty} P_{Ai}}{P_{A0}} \qquad (3)$$

The change of k with the tool feed rate and the tool rake angle is plotted in Fig. 8. The error bars indicate the maximum and the minimum values of k for every three measurements, and the data points show the average value of k. As the tool feed rate is increased from 0.5 to 8 µm/rev, the ratio k gradually increases. However, when the tool feed rate is further increased from 8 µm/rev, the ratio k is almost constant. This indicates that the number of dislodged SiC grains increases with the tool feed rate only when the tool feed rate is low; while at high feed rates, dislodgment of SiC grains is independent of the tool feed rate. Moreover, after the
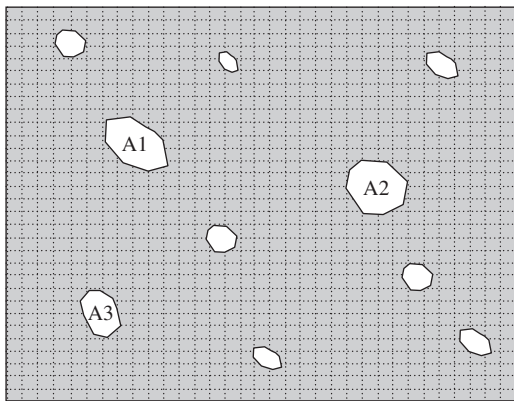

Fig. 7. Schematic diagram of the image processing (pixel counting) method used for calculation of the fracture ratio. A1, A2, A3, etc. indicate microfractures on the machined surface.
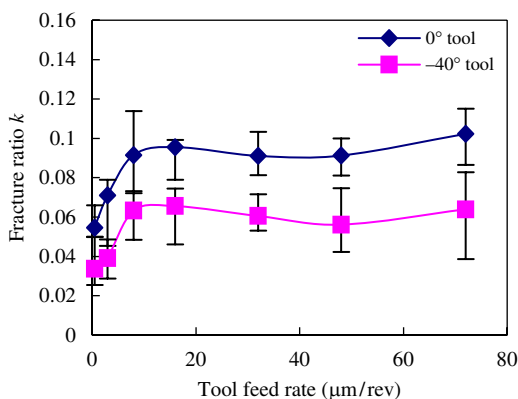

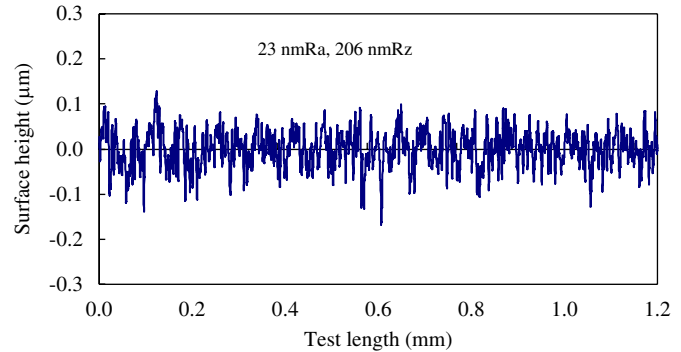**Fig. 8.** Plots of the fracture ratio for different tool rake angles as a function of the tool feed rate.

**Fig. 9.** Profile of a surface machined using −40° rake angle tool at a high tool feed rate of 72 µm/rev.

comparison of the two curves, it is clear that the fracture ratio for the −40° rake angle tool is significantly lower than that of the 0° tool over the total range of tool feed rate. The compressive stress induced by the negative tool rake angle restrains the dislodgement of SiC grains, leading to a smaller fracture ratio.

Fig. 9 shows a profile of the surface machined using −40° tool at conditions: $v = 2000$ rpm; $d = 2$ µm and $f = 72$ µm/rev. The surface roughness is 206 nm Rz (average maximum profile height) and 23 nm Ra (roughness average). The time required to machine the 30 mm radius sample in one cut was only 6 s due to the high tool feed rate. Therefore, a large-radius round tool with a negative rake angle enables precision machining of RB-SiC with very high efficiency. Fig. 10 shows SEM micrographs of the machined surface at different magnifications. The surface is basically smooth but is dotted with micropits. Nevertheless, the size and the number of microfractures evident in Fig. 10 are both smaller than the corresponding ones of those for the sample machined with a tool rake angle of 0° (Fig. 6(b)). This result also indicates that a negative rake angle is useful for reducing grain dislodgements from the machined surface. Additionally, Fig. 10(c) shows that, except for the SiC grain dislodgements, the workpiece material can be completely ductile cut as with metal cutting.

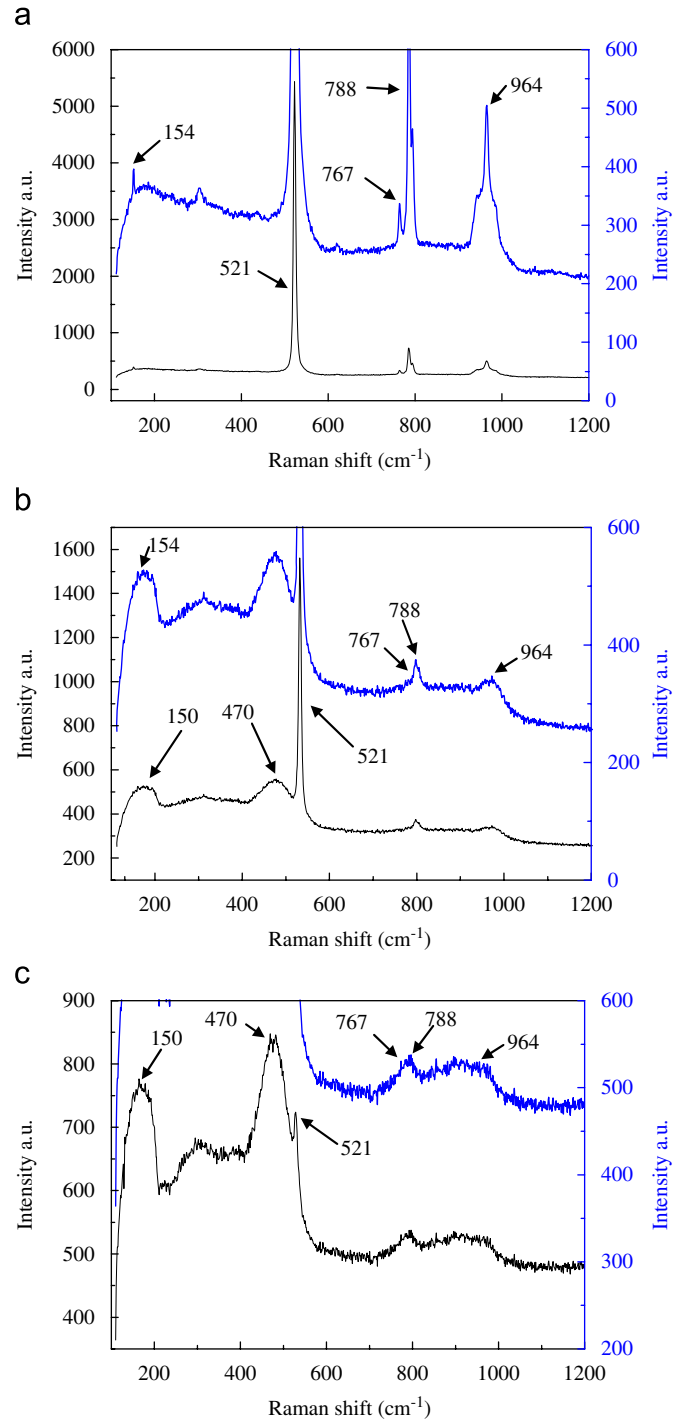### 3.3. Change in material microstructure

The sample surfaces were examined before and after machining using a laser micro-Raman spectrometer to investigate whether phase transformation had occurred during cutting. The grain size of SiC and Si is extremely small (<1 µm), and hence both SiC and Si can be detected by one Raman test, as the nominal spot size of the laser is 1 µm. Fig. 11(a) shows a Raman spectrum of the uncut sample surface (lower curve and left-side intensity scale) and a replot of the same spectrum at a magnified intensity scale (upper curve and right-side intensity scale). There is a strong sharp peak at 521 cm^{-1} that corresponds to crystalline Si (c-Si), and four peaks at 154, 767, 788, and 964 cm^{-1} that correspond to the four characteristic peaks of the 6H-SiC polycrystal [21], which confirms that the RB-SiC sample is composed of crystalline Si and crystalline 6H-SiC.

Figs. 11(b) and (c) show Raman spectra of an area of Si bond on the surface after machining with tools at tool rake angles 0° and −40°. In each graph, the lower curve is the original Raman spectrum and the upper curve is a replot of the same spectrum at a magnified intensity scale. Although a sharp peak still appears at 521 cm^{-1} in Fig. 11(b), two broadband peaks are evident at 470 and 150 cm^{-1}, indicating the presence of amorphous Si (a-Si). This Raman spectrum is very similar to that of ductile machined Si wafers [22,23], which demonstrates that a thin layer of crystalline
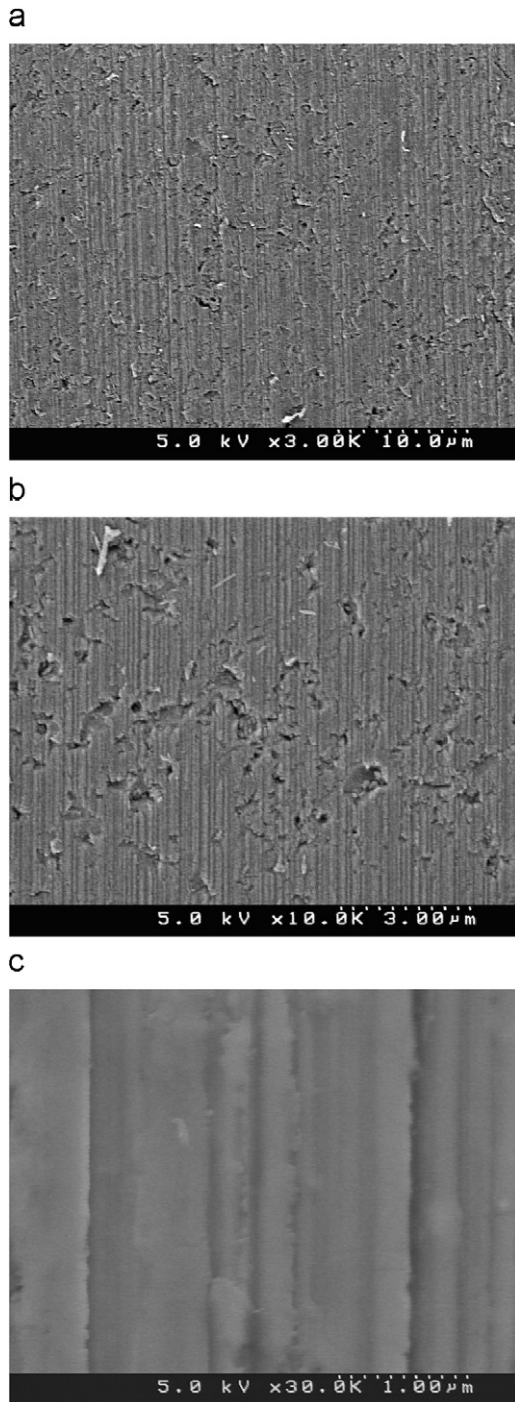
Fig. 10. SEM micrographs of a surface machined with a $-40°$ rake angle tool at a tool feed rate of 72 μm/rev: (a) ×3000; (b) ×10,000; and (c) ×30,000.

Fig. 11. (a) Raman spectrum of the as-received RB-SiC sample, plotted in different scales of intensity. (b) and (c) Raman spectra of sample surfaces machined using diamond tools with rake angles of $0°$ and $-40°$, respectively.

Si has transformed into the amorphous state. In comparison with Fig. 11(b), the broadband peaks centered at 470 and 150 cm^{-1} in Fig. 11(c) have grown significantly, whereas the peak at 521 cm^{-1} has become extremely small. This indicates that a thick layer of Si bond in the RB-SiC sample has changed from crystalline to amorphous phase. That is, a higher negative tool rake angle has a more significant effect on Si amorphization. However, comparison of Fig. 11(a), (b) and (c), does not reveal obvious changes in the positions of the 6H-SiC Raman peaks, although there is a distinct decrease in the intensity of these peaks after machining. These results suggest that 6H-SiC grains do not undergo phase transformation during machining, even if plastic flow occurs.

3.4. Chip formation behavior

The cutting chips were collected and observed using SEM. Fig. 12(a) and (b) shows two pairs of different magnification SEM micrographs of the chips produced by diamond tools of different rake angles $0°$ and $-40°$, respectively. In the low-magnification
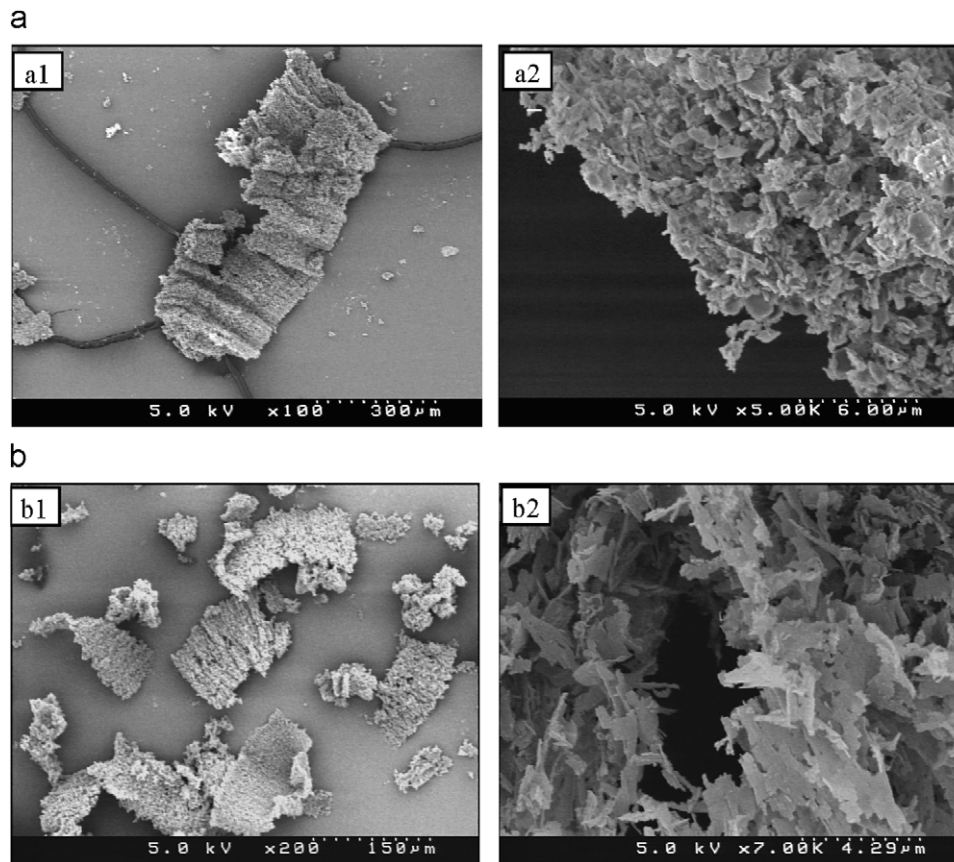
Fig. 12. SEM micrographs of cutting chips generated by diamond tools of different rake angles of (a) $0°$ and (b) $-40°$. Micrographs a1 and b1 are low magnification and a2 and b2 are high magnification.

micrographs a1 and b1, all the chips appear to be continuous and ribbon-like. However, in the high-magnification micrographs a2 and b2, the chips appear to have more separated structures, and there are distinct differences between the structures in a2 and b2. The chip in micrograph a2 consists of numerous microparticles and small flat pieces that are different in size and shape, while the chip in micrograph b2 is composed of extremely thin curled slices. These micrographs suggest that dislodgement of SiC grains dominates the chip formation for a $0°$ tool rake angle (Fig. 12(a)), while ductile cutting of the SiC grains dominates the chip formation for a $-40°$ tool rake angle (Fig. 12(b)), as with metal cutting.

3.5. Tool wear

After machining, the diamond tools were examined using the SEM to evaluate the tool wear patterns. Fig. 13(a) shows the cutting edge of a $0°$ rake angle tool after cutting for 7.2 m at high tool feed rates ($24-72 \mu m/rev$). Numerous microchippings are evident on the cutting edge. It is presumed that these microchippings are caused by microimpacts between the cutting edge and SiC grains. Fig. 13(b) shows the cutting edge of a $-40°$ rake angle tool after cutting for 18.6 m at low tool feed rates ($1-24 \mu m/rev$). There is a uniform wear pattern on the flank face that consists of very fine microgrooves parallel to the cutting direction. This wear pattern is similar to that obtained from the ultraprecision cutting of Si wafers [24], although the total cutting distance in this study is much shorter than that used in Si machining. The groove wear pattern may be caused by the abrasive scratching of SiC grains, and also possibly by thermal-chemical effects.

3.6. Discussion

The mechanism for removal of RB-SiC material can be considered from the deformation behavior of each of the two components: the Si bond and 6H-SiC grains. In Section 3.3, the Raman investigation confirmed that the Si bond undergoes amorphization, which assists the restraint of microfracture formation and facilitates continuous chip formation, due to the ductility of amorphous Si [25]. However, the amount of Si is too small (12%) to dominate the general machining mechanism of RB-SiC.

Therefore, the dominant factor in machining RB-SiC is the mechanical behavior of 6H-SiC grains. High-pressure tests have shown that 6H-SiC crystals do not undergo phase transformation even at hydrostatic pressures up to 95 GPa [26]; in the present study also, no phase transformation was detected in the 6H-SiC grains. Therefore, the deformation of the material is most likely governed by dislocation mobility. It is generally believed that at low temperature, SiC crystals are extremely brittle and cannot be plastically deformed; however, many studies on nanoindentation and abrasive machining of 6H-SiC crystals have shown that even at ambient temperature, plastic deformation can be achieved within a small control volume before fracture occurs [27–29].

When using a round-nosed tool for cutting, the undeformed chip thickness t varies along the cutting edge from zero to t_{max}, thus plastic deformation of 6H-SiC may occur along the tool tip apex where the undeformed chip thickness is less than the critical value for ductile–brittle transition (t_c). As schematically shown in Fig. 14(a), when $t < t_c$, 6H-SiC grains are ductile cut, generating very thin plastically deformed chips, such as those in Fig. 12(b).
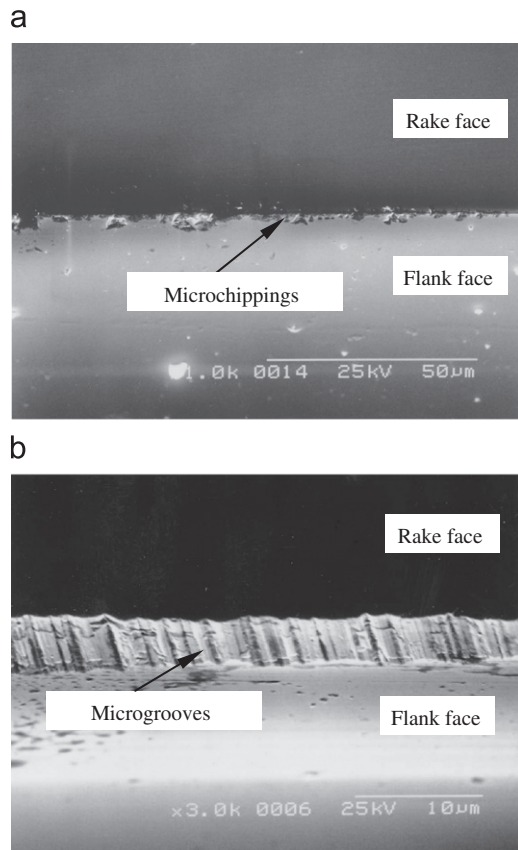
Fig. 13. SEM micrographs of (a) the 0° rake angle tool after cutting for 7.2 m at a high tool feed rate, and (b) the −40° rake angle tool after cutting for 18.6 m at a low tool feed rate.

Fig. 14. Schematic models for material removal during cutting of RB-SiC: (a) ductile cutting when $t < t_c$ and brittle cutting when $t > t_c$; and (b) dislodgement of 6H-SiC grains.

In other words, a few SiC grains will be cut into two parts: one part will be removed as a chip while the other part will remain embedded in the workpiece, and hence a very smooth surface can be obtained. When $t > t_c$, as shown in the upper region in Fig. 14(a), the 6H-SiC grains begin to fracture via cleavage cracks. However, the fracture energy can be released at the grain boundaries, thus the microcracks propagate within the grains and are then stopped at the grain boundaries. As a result, the microcracks depicted in the upper region of Fig. 14(a) do not propagate deeply. This may be the reason why large-scale fractures, such as those observed in cutting single-crystal materials such as Si and Ge, were not observed in the cutting of RB-SiC.

It is noteworthy that not all the 6H-SiC grains can be cut into two parts. A few shallow grains will be dislodged from the surface by the tool tip, leaving micropits on the machined surface, as shown in Fig. 14(b). The dislodgement phenomenon is mainly determined by the bonding strength at the grain boundaries. The mechanism for material removal may also depend on pre-existing defects, such as micropores generated during formation of the material. This suggests that the mechanism for machining of RB-SiC is far more sophisticated than that of single crystalline or amorphous SiC materials.

Another possible factor affecting the mechanism for material removal is thermal effects. Although RB-SiC has excellent thermal stability and its material properties do not change significantly even at very high temperature, thermal effects may become significant in high-speed cutting when a very significant temperature increase occurs in the cutting region. This issue will be investigated in the future.
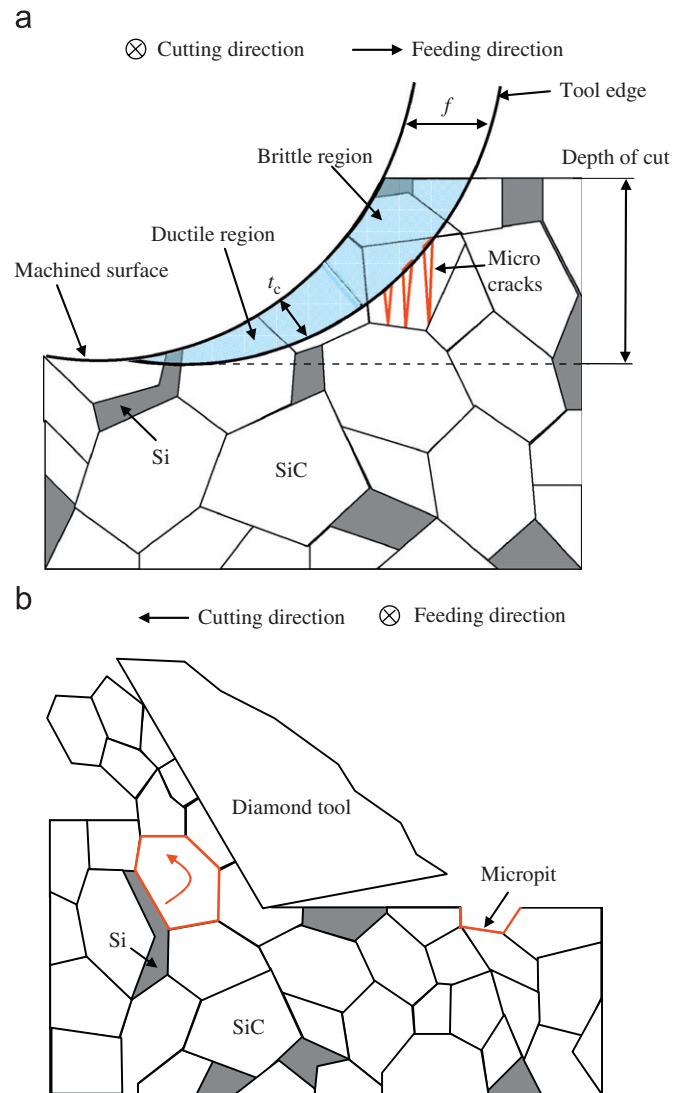
4. Conclusion

RB-SiC ceramics were machined using large-radius round-nosed diamond tools to investigate the mechanism for material removal. The major conclusions are summarized as follows:

(1) The machined surface roughness is not significantly affected by the tool feed rate, but depends mainly on the material microstructure, i.e., grain size. The surface roughness in ductile machining is caused by the dislodgement of a very small amount of 6H-SiC grains.
(2) Raman spectroscopy revealed that the Si bond component underwent amorphization during machining, while no phase transformation was observed for the 6H-SiC grains. The ductile response of the workpiece material originates from the dislocation-based plasticity of 6H-SiC.
(3) The mechanism for removal of the SiC grains involves ductile cutting, cleavage cracking and grain dislodgement. The material removal behavior depends on the size and depth of the SiC grains and the bonding strength at the grain boundaries.

(4) Large-scale fractures do not occur during cutting of RB-SiC, due to the ductile response of the Si bond and fracture energy releasing effects at the grain boundaries. This feature enables the precision machining of RB-SiC at a very high material removal rate.

(5) Tool wear can be classified into two types: One is the microchipping that occurs on zero rake angle tools under high feed conditions; the other is microgrooved flank wear that occurs for highly negative rake angle tools under feed conditions.

Acknowledgements

References

[1] C. Hall, M. Tricard, H. Murakoshi, Y. Yamamoto, K. Kuriyama, H. Yoko, New mold manufacturing techniques, Proceedings of the SPIE 5868 (2005) 58680V.

[2] S. Suyama, T. Kameda, Y. Itoh, Development of high-strength reaction-sintered silicon carbide, Diamond and Related Materials 12 (2003) 1201–1204.

[3] S. Suyama, Y. Itoh, K. Tsuno, K. Ohno, Φ650 mm optical space mirror substrate of high-strength reaction-sintered silicon carbide, Proceedings of SPIE 5868 (2005) 58680E.

[4] H. Toshiya, I. Ichiro, S. Junichi, Grinding of silicon carbide with diamond wheel, Transactions of the Japan Society of Mechanical Engineers C 51 (1985) 1864–1870.

[5] Y. Dai, H. Ohmori, W. Lin, H. Eto, N. Ebizuka, K. Tsuno, ELID grinding properties of high-strength reaction-sintered SiC, Key Engineering Materials 291–292 (2005) 121–126.

[6] H.Y. Tam, H.B. Cheng, Y.W. Wang, Removal rate and surface roughness in the lapping and polishing of RB-SiC optical components, Journal of Materials Processing Technology 192–193 (2007) 276–280.

[7] H. Cheng, Z. Feng, S. Lei, Y. Wang, Magnetorheological finishing of SiC aspheric mirrors, Materials and Manufacturing Processes 20 (6) (2005) 917–931.

[8] H. Kitahara, Y. Noda, F. Yoshida, H. Nakashima, N. Shinohara, H. Abe, Mechanical behavior of single crystalline and polycrystalline silicon carbides evaluated by Vickers indentation, Journal of the Ceramic Society of Japan 109 (2001) 602–606.

[9] T. Nakasuji, S. Kodera, S. Hara, H. Matsunaga, N. Ikawa, S. Shimada, Diamond turning of brittle materials for optical components, Annals of the CIRP 39 (1990) 89–92.

[10] P.N. Blake, R.O. Scattergood, Diamond turning of brittle materials for optical components, Journal of the American Ceramic Society 73 (1990) 949–957.

[11] J. Yan, K. Syoji, T. Kuriyagawa, H. Suzuki, Ductile regime turning at large tool feed, Journal of Materials Processing Technology 121 (2002) 363–372.

[12] J. Yan, K. Maekawa, J. Tamaki, T. Kuriyagawa, Micro grooving on single-crystal germanium for infrared Fresnel lenses, Journal of Micromechanics and Microengineering 15 (2005) 1925–1931.

[13] T. Ohta, J. Yan, S. Yajima, Y. Takahashi, N. Horikawa, T. Kuriyagawa, High-efficiency machining of single-crystal germanium using large-radius diamond tools, International Journal of Surface Science and Engineering 1 (2007) 374–392.

[14] J. Patten, W. Gao, K. Yasuto, Ductile regime nanomachining of single-crystal silicon carbide, ASME Journal of Manufacturing Science and Engineering 127 (2005) 522–532.

[15] B. Bhattacharya, J. Patten, J. Jacob, Single point diamond turning of CVD coated silicon carbide, in: Proceedings of 2006 ASME International Conference on Manufacturing Science and Engineering, October 8–11, Ypsilanti, Michigan, USA, 2006, pp. 1–6.

[16] J.P. Davim, José Silva, A.M. Baptista, Experimental cutting model of metal matrix composites (MMCs), Journal of Materials Processing Technology 183 (2007) 358–362.

[17] Y. Wang, L.J. Yang, N. Wang, An investigation of laser-assisted machining of Al_2O_3 particle reinforced aluminum matrix composite, Journal of Materials Processing Technology 129 (2002) 268–272.

[18] T. Ozben, E. Kilickap, O. Cakır, Investigation of mechanical and machinability properties of SiC particle reinforced Al-MMC, Journal of Materials Processing Technology 198 (2008) 220–225.

[19] Y.F. Ge, J.H. Xu, H. Yang, S.B. Luo, Y.C. Fu, Workpiece surface quality when ultra-precision turning of SiCp/Al composites, Journal of Materials Processing Technology 203 (2008) 166–175.

[20] J. Yan, M. Yoshino, T. Kuriyagawa, T. Shirakashi, K. Syoji, R. Komanduri, On the ductile machining of silicon for micro electro-mechanical systems (MEMS), opto-electronic and optical applications, Materials Science and Engineering A 297 (2001) 230–234.

[21] S. Nakashima, H. Harima, Raman investigation of SiC polytypes, Physica Status Solidi A 162 (1997) 39–64.

[22] J. Yan, Laser micro-Raman spectroscopy of single-point diamond machined silicon substrates, Journal of Applied Physics 95 (4) (2004) 2094–2101.

[23] J. Yan, T. Asami, T. Kuriyagawa, Nondestructive measurement of the machining-induced amorphous layers in single-crystal silicon by laser micro-Raman spectroscopy, Precision Engineering 32 (2008) 186–195.

[24] J. Yan, K. Syoji, J. Tamaki, Some observations on the wear of diamond tools in ultra-precision cutting of single-crystal silicon, Wear 255 (2003) 1380–1387.

[25] J. Yan, H. Takahashi, J. Tamaki, X. Gai, T. Kuriyagawa, Transmission electron microscopic observation of nanoindentations made on ductile-machined silicon wafers, Applied Physics Letters 87 (2005) 211901.

[26] M. Yoshida, A. Onodera, M. Ueno, K. Takemura, O. Shimomura, Pressure-induced phase transition in SiC, Physical Review B 48 (1993) 10587–10590.

[27] L. Yin, E.Y.J. Vancoille, K. Ramesh, H. Huang, Surface characterization of 6H-SiC (0 0 0 1) substrates in indentation and abrasive machining, International Journal of Machine Tools and Manufacture 44 (2004) 607–615.

[28] S. Shim, J. Jang, G.M. Pharr, Extraction of flow properties of single-crystal silicon carbide by nanoindentation and finite-element simulation, Acta Materialia 56 (2008) 3824–3832.

[29] J.R. Grim, M. Benamara, M. Skowronski, W.J. Everson, V.D. Heydemann, Transmission electron microscopy analysis of mechanical polishing-related damage in silicon carbide wafers, Semiconductor Science and Technology 21 (2006) 1709–1713.